NASA/TP-2019-220320

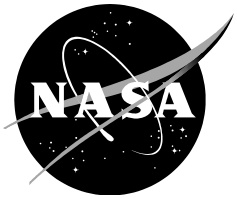

Data Validation: Difference Imaging and Centroid Analysis

Joseph Twicken
Ames Research Center, Moffett Blvd, Mountain View, CA 94040

August, 2019

NASA STI Program ... in Profile

Since its founding, NASA has been dedicated to the advancement of aeronautics and space science. The NASA scientific and technical information (STI) program plays a key part in helping NASA maintain this important role.

The NASA STI program operates under the auspices of the Agency Chief Information Officer. It collects, organizes, provides for archiving, and disseminates NASA's STI. The NASA STI program provides access to the NTRS Registered and its public interface, the NASA Technical Reports Server, thus providing one of the largest collections of aeronautical and space science STI in the world. Results are published in both non-NASA channels and by NASA in the NASA STI Report Series, which includes the following report types:

- TECHNICAL PUBLICATION. Reports of completed research or a major significant phase of research that present the results of NASA Programs and include extensive data or theoretical analysis. Includes compilations of significant scientific and technical data and information deemed to be of continuing reference value. NASA counterpart of peer-reviewed formal professional papers but has less stringent limitations on manuscript length and extent of graphic presentations.

- TECHNICAL MEMORANDUM. Scientific and technical findings that are preliminary or of specialized interest, e.g., quick release reports, working papers, and bibliographies that contain minimal annotation. Does not contain extensive analysis.

- CONTRACTOR REPORT. Scientific and technical findings by NASA-sponsored contractors and grantees.

- CONFERENCE PUBLICATION. Collected papers from scientific and technical conferences, symposia, seminars, or other meetings sponsored or co-sponsored by NASA.

- SPECIAL PUBLICATION. Scientific, technical, or historical information from NASA programs, projects, and missions, often concerned with subjects having substantial public interest.

- TECHNICAL TRANSLATION. English-language translations of foreign scientific and technical material pertinent to NASA's mission.

Specialized services also include organizing and publishing research results, distributing specialized research announcements and feeds, providing information desk and personal search support, and enabling data exchange services.

For more information about the NASA STI program, see the following:

- Access the NASA STI program home page at http://www.sti.nasa.gov

- E-mail your question to help@sti.nasa.gov

- Phone the NASA STI Information Desk at 757-864-9658

- Write to:
  NASA STI Information Desk
  Mail Stop 148
  NASA Langley Research Center
  Hampton, VA 23681-2199

NASA/TP-2019-220320

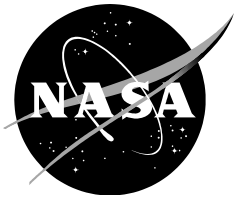

Data Validation: Difference Imaging and Centroid Analysis

Joseph Twicken
Ames Research Center, Moffett Blvd, Mountain View, CA 94040

National Aeronautics and
Space Administration

Ames Research Center
Moffett Blvd, Mountain View, CA 94040

August, 2019

KPO @ AMES DESIGN NOTE

Design Note No.: KADN-26302

Title: Data Validation: Difference Imaging and Centroid Analysis

Author: Joseph Twicken Signature: _____

GS SE Approval: Todd Klaus Signature: _____

Science Approval: Jon Jenkins Signature: _____

Distribution: N/A

Revision History:

Rev. Letter	Revision Description	Date	Author/Initials
-	Draft	21 Nov 2011	JDT
	Initial Revision	07 Dec 2011	JDT

Overview:

This Design Note describes the theory and application of difference imaging for automated validation of planet candidates in the Data Validation (DV) CSCI. This is one of the diagnostic tools employed in DV for planet candidate validation. The other DV diagnostics are described in separate KADNs and in the reference documents listed below. This document describes the difference image generation process, PRF-based centroiding of the out-of-transit and difference images, computation of quarterly centroid offsets and associated uncertainties, and determination of robust weighted mean centroid offsets/uncertainties over all available quarterly data sets.

PRF-based centroiding is performed with calls to a library of functions that is shared with the Photometric Analysis (PA) and Photometer Data Quality (PDQ) CSCIs. The centroiding library will be the subject of a separate Design Note.

Recommendations:

Difference imaging and analysis of the resulting centroid offsets is a powerful tool for validation of planet candidates. Automated generation of difference images, computation of centroids and centroid offsets, and statistical offset analysis are very efficiently performed in the SOC Pipeline. I recommend that this DV diagnostic tool and others continue to evolve and reflect the latest methods of the Kepler Science Office and Science Team for validation of planet candidates because it is significantly more efficient to provide this functionality within the context of the SOC Pipeline than it is outside of the Pipeline.

Reference Documents

1. J. Jenkins	Algorithm Theoretical Basis Document for the Science Operations Center, KSOC-21008-001, July 2004
2. H. Wu, et al.	Data Validation in the Kepler Science Operations Center Pipeline, Proc. SPIE 7740, 774019, 1-12, 2010
3. P. Tenenbaum, et al.	An Algorithm for the Fitting of Planet Models to Kepler Light Curves, *Proc. SPIE 7740*, 77400J, 1-12, 2010
4. S. Bryson, et al.	The Kepler Pixel Response Function, Astrophysical Journal Letters, 713 (2), L97-102, 2010

Applicable Documents

1. J. Twicken, et al.	KSOC-21072-001, Data Validation SDD
2. P. Tenenbaum	KADN-26268, Data Validation: Design of Fitting Algorithm
3. J. Jenkins	KADN-26083, Data Validation: Centroiding for Transiting Planets

4. B. Clarke — KADN-26284, Data Validation: Centroid Test Implementation
5. J. Li — KADN-26274, Data Validation: Eclipsing Binary Discrimination Tests
6. H. Wu, H. Chandrasekaran — KADN-26069, Bootstrap Algorithm for Establishing Statistical Confidence in Transit Detection
7. P. Tenenbaum, S. Seader — KADN-26288, Transiting Planet Search Science Algorithms
8. J. Twicken — KADN-26272, Photometric Analysis Science Algorithms

Open Items/Action Required

None.

TBDs/TBRs

Paragraph	TBD Item

1. Introduction

This Design Note describes the use of a difference imaging technique for automated validation of planet candidates in the Data Validation (DV) CSCI of the Kepler SOC Pipeline. Planet candidates are first identified when long cadence corrected flux light curves are processed in the Transiting Planet Search (TPS) CSCI. All targets for which a Threshold Crossing Event (TCE) is generated are subsequently processed in DV. A transiting planet model is fitted in DV to the light curve for each target, and a search for additional planets is conducted by repeating the transit search on the residual light curve after the model flux has been removed. The multiple planet search is conducted by calling TPS directly at the Matlab controller level. The fitting of transiting planet models and the search for additional planet candidates is repeated until all planet candidates have been identified for each given DV target. Hundreds of multiple transiting planet systems have already been identified based on analysis of data from observing quarters Q1-8.

A suite of automated tests is performed on all planet candidates in DV to aid in the discrimination between true planet candidates and false positive detections. SOC build 6.1 included the initial release of DV. In subsequent DV releases, difference imaging functionality has been implemented to enhance the validation process. This technique aims to locate the source of a transit signature in the photometric mask of a given target, and to estimate the offset between the transit source and the target itself. Robust and reliable identification of the transit source location is critically important because it reduces expenditure of limited resources (including time and money) on ground based follow-up of false positives. Difference imaging can identify the location of a transit source because it exploits the spatial information in the pixel time series associated with a given target that is not available in the flux time series.

Difference imaging is proving to be a powerful diagnostic for identifying astrophysical false positive detections due to background eclipsing binaries. It is also valuable for identifying the true transit source in crowded apertures. Difference images, centroids and centroid offsets are computed on a target table (i.e. quarterly) basis for each planet candidate. The offsets are then averaged in a robust fashion over multiple quarters to improve the accuracy of the diagnostic. The robust averaging includes weighting based on inverse uncertainties to emphasize centroid offsets with relatively small uncertainties and deemphasize those with relatively large uncertainties.

For each planet candidate, mean in- and out-of-transit images are constructed by averaging the flux in and near each transit on a per pixel basis, and then by averaging over all transits for the given observing quarter. In- and out-of-transit cadences are identified through the transiting planet model that is fitted to the target light curve in the front end of DV. A difference image is generated by subtracting the mean in-transit flux value for each pixel from the mean out-of-transit flux value. Data gaps are ignored in construction of the quarterly images. The numbers of valid and gapped in- and out-of-transit cadences are included in the DV output structure for each target, planet candidate and target table and in figure captions in the DV report.

Transits are excluded from the respective images if the associated in- or out-of-transit cadences overlap (1) the transit of another planet candidate for the given target, (2) a known spacecraft anomaly (e.g. Earth-point for data downlink, safe mode, attitude tweak, and multiple-cadence loss of fine point), or (3) the start or end of the unit of work. A module parameter specifies the period following thermal events (Earth-point and safe mode) during which transits are excluded from difference image generation.

The photocenters of the out-of-transit and difference images are computed by fitting the appropriate Pixel Response Function (PRF) for the given channel. The out-of-transit centroid locates the target, subject to aperture crowding. The difference image centroid precisely locates the source of the transit signature (which may or may not be the given target). The quarterly offsets between out-of-transit and difference image centroids provide both absolute and statistical measures of the separation between target and transit source.

The offset is also computed per planet candidate and observing quarter between the difference image centroid and the target location specified by its Kepler Input Catalog (KIC) celestial coordinates. The offset from the KIC reference position is not subject to aperture crowding but is subject to centroid bias. Robust mean centroid offsets are computed in right ascension and declination with associated uncertainties for the difference image centroids relative to the quarterly out-of-transit centroids and relative to the KIC coordinates of the given target.

The DV difference imaging and centroid analysis methodology is described in Section 2 of this document. Module parameters relevant to difference image generation and analysis of the centroid offsets are defined in Section 3. Derivations describing the formulation of the difference images and the computation of the centroid offsets are presented in Section 4.

2. Methodology

The difference imaging and centroid analysis methodology is presented in this section. An overview is presented in 2.1. The difference image generation process is described in 2.2. The difference image centroid and offset analysis algorithms are discussed in 2.3. Propagation of uncertainties is essential for assessing the significance of the difference images and centroid offsets; it is described where applicable.

2.1 Overview

TPS and DV form the heart of the Kepler Science Processing Pipeline. These CSCIs operate on multi-quarter light curves with computationally intensive algorithms to search for transiting planets, model their orbital parameters, and validate the planet candidates. The complexity of the folding algorithm in TPS increases with the square of the amount of available data. TPS and DV were ported to the NASA Advanced Supercomputer (NAS) facility in the SOC 7.0 build where they run on Pleiades. It should be noted that DV calls TPS directly at the Matlab controller level as part of the multiple planet search. As the number of quarterly data sets increases then the fraction of DV run time spent searching for transiting planets will also increase.

A block diagram of DV is illustrated in Figure 1. Pixel and flux time series are preprocessed in preparation for multi-quarter transiting planet search and model fitting and the diagnostic tests that follow. From the standpoint of difference image generation, it should be noted that the preprocessing steps include (1) gapping of all calibrated pixel time series on known anomaly cadences (including the Argabrightening cadences identified for each module output in PA), (2) removal of the cosmic rays identified in PA from the quarterly pixel time series, and (3) removal of background flux per pixel and cadence based on two-dimensional polynomials fitted to the long cadence background pixels in PA. After the preprocessing steps have been completed, ancillary data are synchronized to the long cadence timestamps quarter by quarter to support the correction of systematic errors in pixel, flux and centroid time series. Transiting planet model fitting is performed in the whitened domain in an iterative fashion. Once the fit for a given planet candidate has converged, the model light curve is removed from the corrected flux time series and the residual is searched to identify additional transiting planet candidates. The process is repeated until all candidates have been identified for the target in question.

A suite of diagnostic tests and analyses are performed in the back-end of DV after all planet candidates have been identified and fitted. Collectively, these diagnostics aim to differentiate between true planet candidates and astrophysical false positive detections. Difference imaging and centroid analysis is the subject of this document. Other DV diagnostics include a centroid motion test, pixel correlation tests, eclipsing binary discrimination tests and a statistical bootstrap. The planet model fitting algorithm and each of the other diagnostic tests are subjects of their own Design Notes referenced in the Applicable Documents section of this document. Results of the transiting planet model fits and diagnostic tests are passed from Matlab to Java

through the DV module interface and persisted in the Kepler file store. Results are also displayed in dashboards, tables and diagnostic figures in an extensive report generated for each DV target in PDF format.

It should be noted that PRF-based centroiding and centroid offset analysis are performed on the pixel correlation images generated per planet candidate and target table in DV in the same fashion as they are performed on the difference images. Quarterly pixel correlation image centroid offsets and robust averages are included in the DV output structure and report.

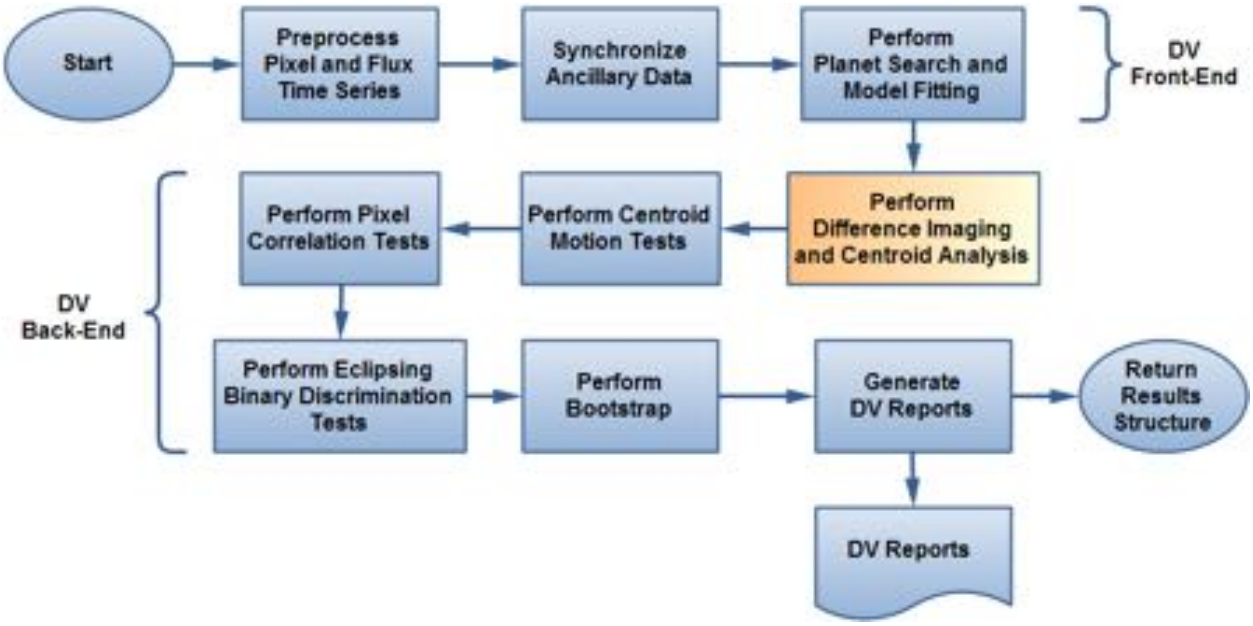

Figure 1: DV block diagram. The front-end of DV includes time series preprocessing, ancillary data synchronization and multiple planet search/model fitting. The DV back-end includes a suite of diagnostic tests and analyses to differentiate between true planet candidates and false positive detections. The DV unit of work may include multiple quarterly data sets for one or more targets with TPS TCEs.

2.2 Difference Image Generation

In-transit, out-of-transit and difference images are generated for each DV target, planet candidate and target table (i.e. quarter) as long as (1) the transiting planet model fit for the given planet candidate converged successfully, and (2) there are one or more *clean* transits for the planet candidate in the given target table. A clean transit is one which occurred during a period when valid science data were collected and which is not excluded from the difference imaging process for one of the reasons to be enumerated later. DV produces a so-called *direct* image displaying the mean flux per pixel over the duration of the target table in the event that a difference image cannot be generated for a given planet candidate and target table.

The difference image generation process is shown at a high level in Figure 2. The iterations over targets, target tables and planet candidates are illustrated. Functional blocks in the diagram will be referenced with bold type where they are discussed in the following text.

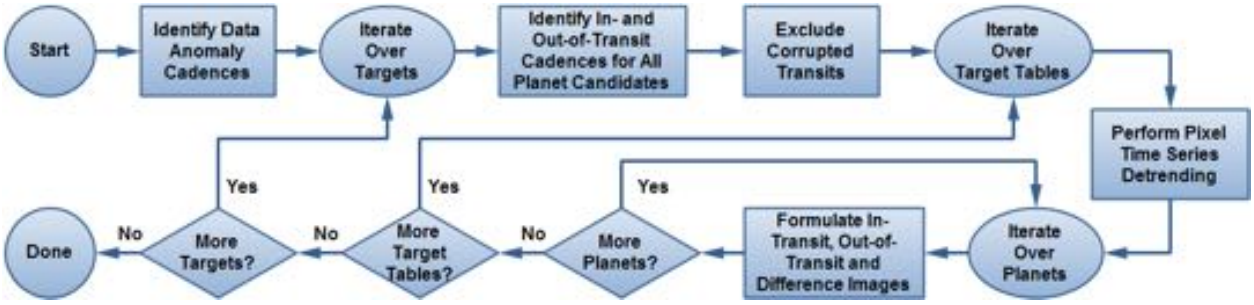

Figure 2: High-level representation of the difference image generation process. In-transit, out-of-transit, and difference images are generated (where possible) for each DV target, planet candidate and target table (i.e. quarter). Pixel time series detrending prior to formulation of the respective images is optional, and disabled by default in the SOC 8.0 Pipeline.

Identify Data Anomaly Cadences. The Pipeline data anomaly flags are parsed, and data anomaly cadences are defined to include the following:

- Earth-points, including a specified post-anomaly extension (DV 8.0 default = 1 day)
- Safe modes, including a specified post-anomaly extension (DV 8.0 default = 1 day)
- Attitude tweaks
- Multi-cadence coarse-points
- Exclude cadences
- First cadence in unit of work (to exclude partial transits)
- Last cadence in unit of work (to exclude partial transits)

As described later, transits are excluded from the difference image generation process if the associated in- or out-of-transit cadences coincide with one or more of the data anomaly cadences listed above.

Identify In- and Out-of-Transit Cadences for All Planet Candidates. For each DV target, the in- and out-of-transit cadences are identified for all planet candidates over the duration of the unit of work. These cadences are identified by generating the model light curve for each planet candidate on the barycentric-corrected timestamp for each cadence based on the parameter values of the respective planet model fits (to all transits). In-transit cadences are defined as those for which the transit depth exceeds a specified fraction (DV 8.0 default = 0.75) of the maximum depth. Out-of-transit (*control*) cadences are defined as those sequences of cadences preceding and following each transit with a duration equal in width to the transit duration derived

from the model fit. A buffer (DV 8.0 default = 3 cadences) is specified to isolate the control cadences from the transit events and preserve the integrity of the difference images in the event that the planet model fit is imperfect.

Figure 3 illustrates one transit of HAT-P-7b (KID 10666592) based on the DV planet model fit to all transits. The in-transit cadences are marked in red. The out-of-transit control cadences are marked in green. Three-cadence buffers isolating the control cadences from the transit itself are evident preceding and following the transit. The mean out-of-transit flux level is computed for each transit by averaging the flux values on the associated out-of-transit cadences for all pixels in the target mask; likewise the mean in-transit flux level is computed for each transit by averaging the flux on the associated in-transit cadences for all pixels in the target mask.

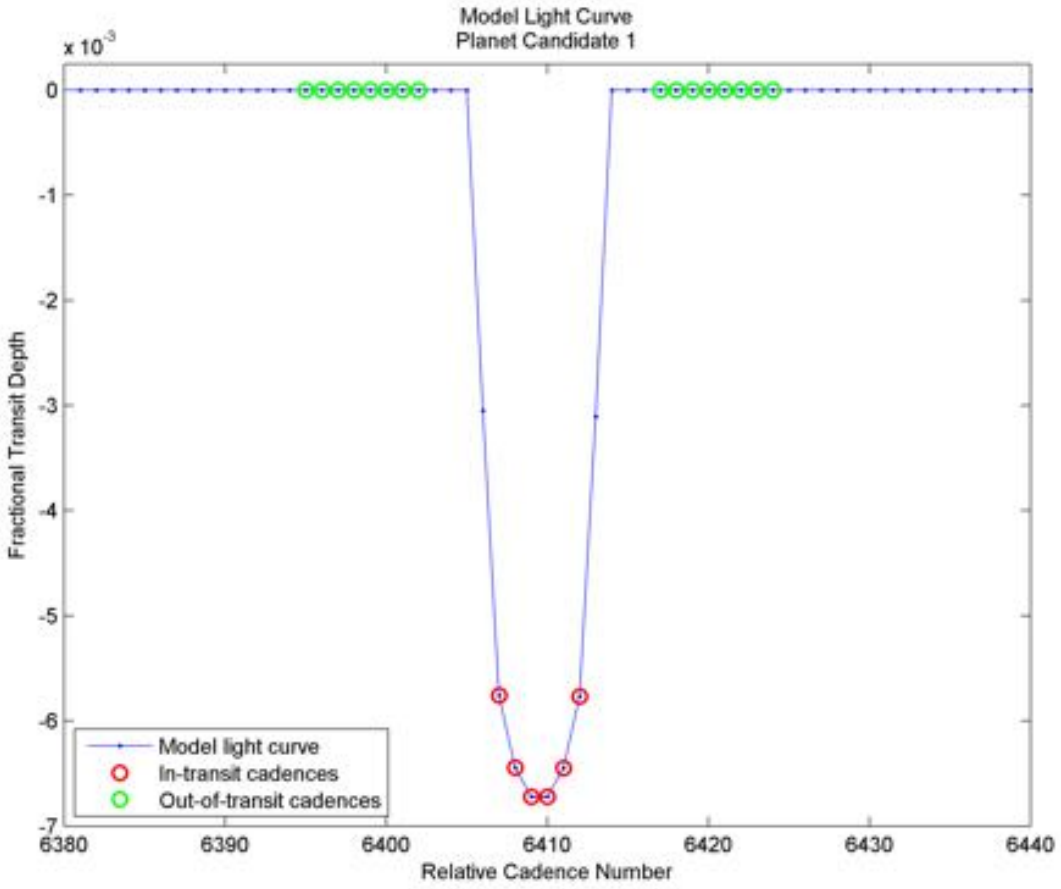

Figure 3: The model light curve illustrating one transit of HAT-P-7b based on the DV planet model fit is shown in blue. In-transit cadences for the purpose of difference image generation are marked in red; these are the cadences for which the transit depth exceeds 75% of the maximum. Out-of-transit cadences for the purpose of difference image generation are marked in green; the control segments preceding and

following the transit are equal in width to the transit duration and isolated from the transit event by a three-cadence buffer.

Exclude Corrupted Transits. Transits corrupted by known data anomalies or by the transits of other planet candidates associated with the same target are excluded from the difference image generation process. This is to prevent compromising the quality and integrity of the difference image. Uncertainties in the resulting difference image values are larger than they otherwise would be if the corrupted transits were not excluded (because the averaging is performed over fewer transit events), but the difference image values are more accurate if the impacted transits are excluded.

Identification of the cadences with known data anomalies has been discussed earlier. Transits are excluded from difference image generation if **any cadence** between the first and last out-of-transit control cadence (inclusively) is coincident with at least one of the (1) known data anomaly cadences, or (2) transit or associated buffer cadences for another planet candidate associated with the given target. Note that transits are **not** excluded from difference image generation if they are only coincident with the out-of-transit cadences of another planet candidate for the given target.

An example of a transit that is excluded from difference image generation because it coincides with a known data anomaly is shown in Figure 4. Here, one transit of Kepler-11c (KID 6541920) overlaps a photometer coarse-point period late in Q2. The coarse-point cadences are marked with magenta squares. In- and out-of-transit cadences that would have been utilized for difference image generation are marked in red and green respectively.

An example of a transit that is excluded from difference image generation because it overlaps the transit of another planet candidate for the same target is shown in Figure 5. Here, one transit of Kepler-11c overlaps a transit of Kepler-11f. The model light curve for Kepler-11c is shown in blue and for Kepler-11f is shown with a red dashed line. In- and out-of-transit cadences that would have been utilized for generating the Kepler-11c difference image are marked in red and green respectively.

An example of a transit that is excluded from difference image generation because its out-of-transit control cadences overlap the transit of another planet candidate for the same target is shown in Figure 6. Here, the control cadences associated with one transit of Kepler-11c overlap a transit of Kepler-11b. The model light curve for Kepler-11c is shown in blue and for Kepler-11b is shown with a red dashed line. In- and out-of-transit cadences that would have been utilized for generating the Kepler-11c difference image are marked in red and green respectively.

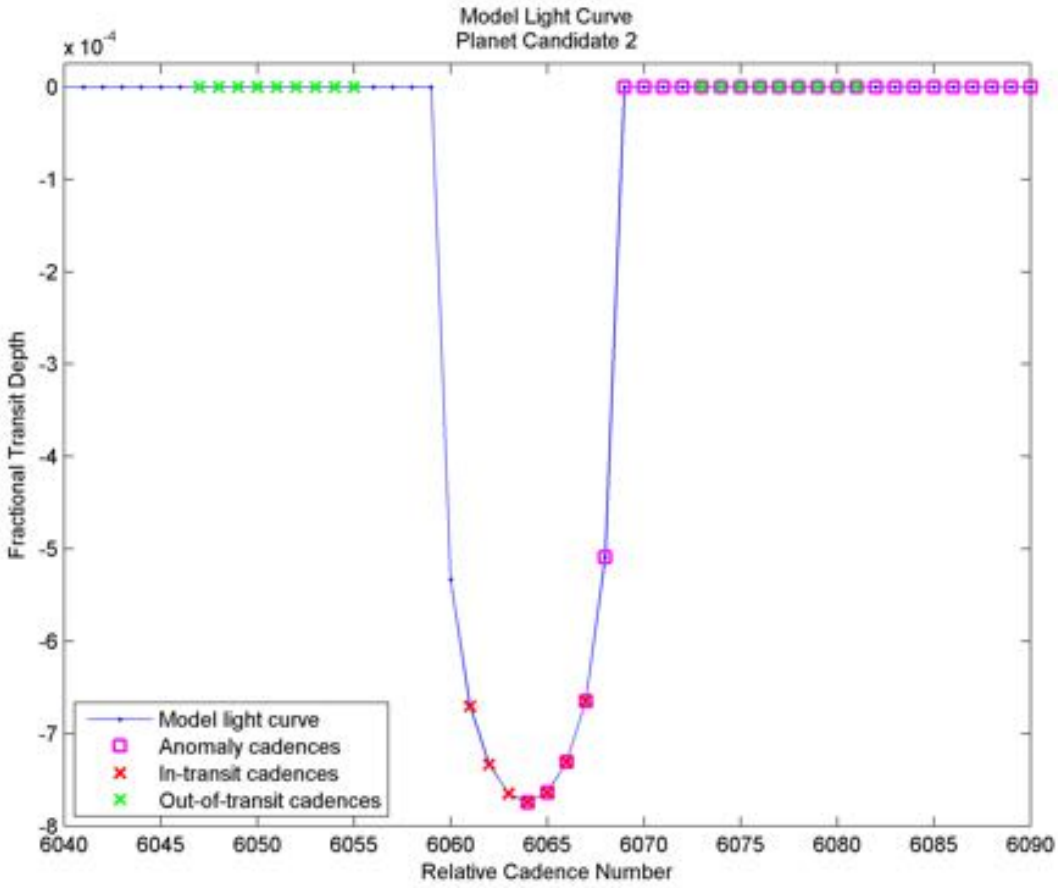

Figure 4: The model light curve illustrating one transit of Kepler-11c based on the DV planet model fit is shown in blue. Cadences associated with a photometer coarse-point event late in Q2 are marked in magenta. In- and out-of-transit cadences that would have been utilized for difference image generation are marked in red and green respectively. This transit is excluded from the difference image generation process because it is coincident with the coarse-point event.

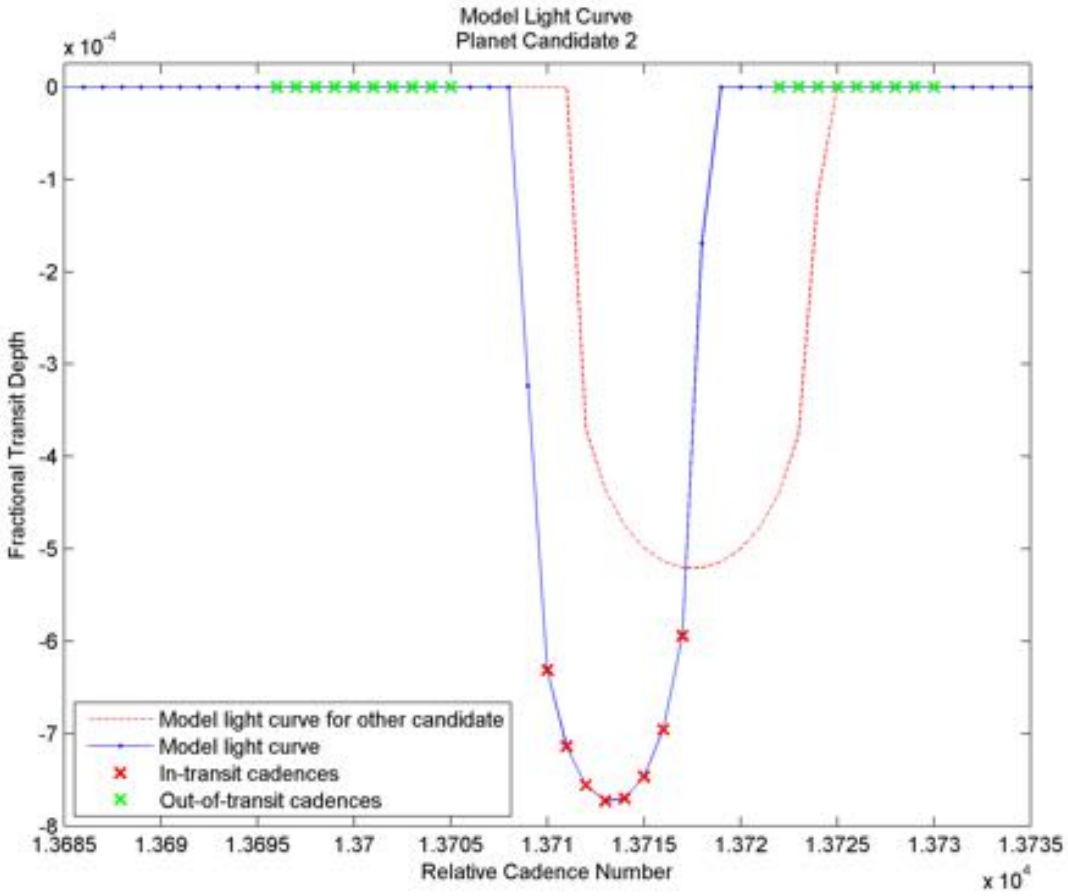

Figure 5: The model light curve illustrating one transit of Kepler-11c based on the DV planet model fit is shown in blue. The model light curve illustrating one transit of Kepler-11f is shown with a red dashed line. In- and out-of-transit cadences that would have been utilized for generating the Kepler-11c difference image are marked in red and green respectively. This transit is excluded from the difference image generation process because it overlaps the transit of another planet candidate associated with the same target.

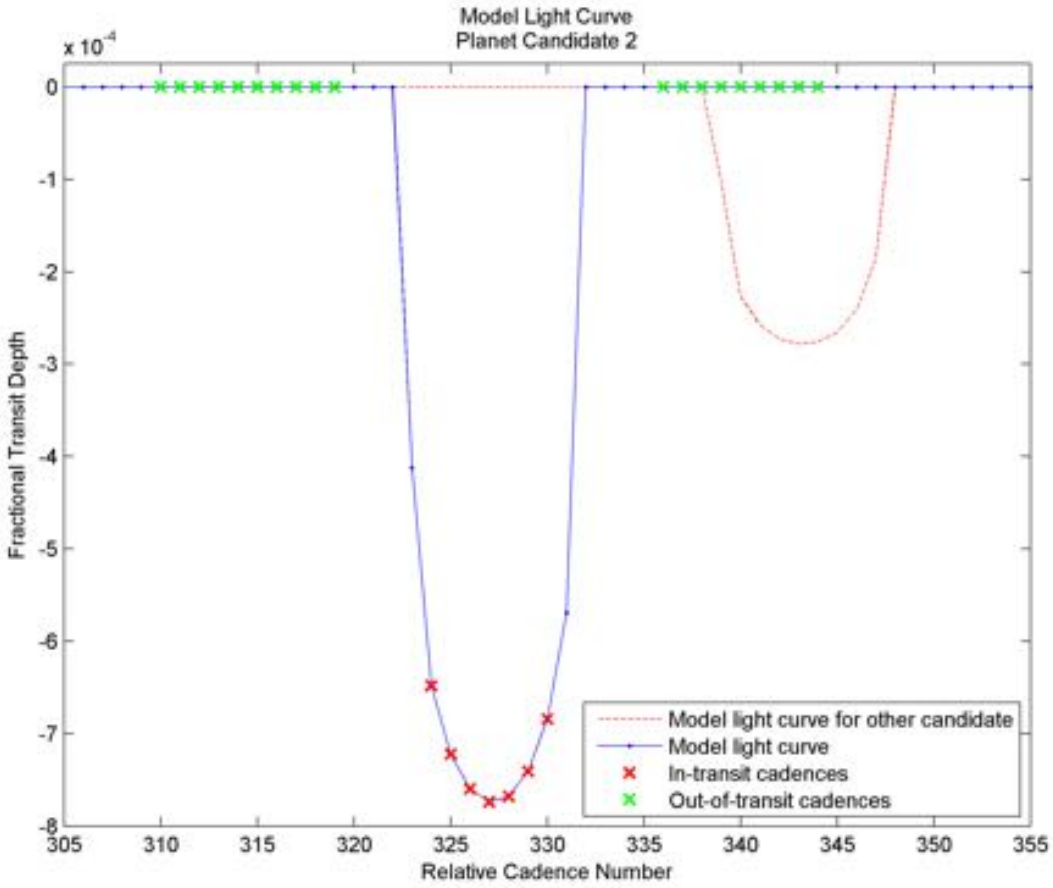

Figure 6: The model light curve illustrating one transit of Kepler-11c based on the DV planet model fit is shown in blue. The model light curve illustrating one transit of Kepler-11b is shown with a red dashed line. In- and out-of-transit cadences that would have been utilized for generating the Kepler-11c difference image are marked in red and green respectively. This transit is excluded from the difference image generation process because it overlaps the transit of another planet candidate associated with the same target.

Perform Pixel Time Series Detrending. Detrending was performed on all pixel time series associated with each target and target table prior to formulation of the difference images when the difference imaging functionality was first incorporated in DV (SOC release 6.2). Science Office and Science Team members subsequently expressed their desire, however, that detrending not be performed by default in later DV releases. Their motivation was to preserve the native transit signatures to the greatest extent possible by eliminating the filtering applied to each pixel time series. Detrending remains an option, but is disabled by default in DV 8.0. For the sake of completeness, the process will be briefly described here.

The pixel time series detrending process is illustrated in Figure 7**.** The length of the median smoothing filter is selected based on the maximum transit duration and minimum orbital period for all planet candidates associated with the given target. Specifically, the median filter length is determined by the square root of the maximum transit duration in cadences and the minimum orbital period in cadences although the filter length must be odd and cannot exceed the length of the target table in question. The median filter length is set to a specified default (DV 8.0 default = 73 cadences) if the planet model fit is unsuccessful for all planet candidates.

Each pixel time series is initially detrended with a specified low order polynomial (DV 8.0 default = 2) and gaps are then filled by linear interpolation. Polynomial detrending reduces the edge effects for the median filtering that follows. A median filter is applied to smooth all of the interpolated pixel time series, and the residual time series (interpolated minus smoothed) is computed. Finally, the median value of each of the original time series is restored to all cadences of the respective detrended time series. Detrending each pixel time series in this fashion removes trends in the data on time scales that are long compared to the length of the median filter.

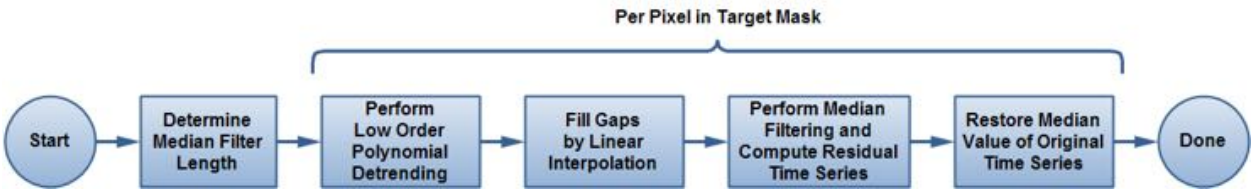

Figure 7: The pixel time series detrending process. Detrending is performed optionally in the SOC pipeline and is disabled by default in DV 8.0. After selecting the median filter length, the process is applied in parallel to all pixel time series associated with the given target.

Formulate Difference Images. In-transit, out-of-transit and difference images are generated for each DV target, target table (quarter) and planet candidate as long as (1) the transiting planet model fit for the given planet candidate converged successfully, and (2) there are one or more clean transits for the planet candidate in the given target table. A direct image displaying the mean flux per pixel over the duration of the target table is produced in the event that a difference image cannot be generated for a given planet candidate and target table.

The process for formulating the mean in-transit, mean out-of-transit and difference images is illustrated in Figure 8. It is applied in parallel for all pixels in the aperture mask associated with the given target. The in- and out-of-transit cadences associated with each of the transits that have not been excluded as described earlier are retrieved for the given target table and planet candidate. For each transit, the mean in-transit flux value is computed by averaging the pixel values over the in-transit cadences and the mean out-of-transit flux value is computed by averaging the pixel values over the out-of-transit control cadences. Gapped pixel values are ignored for the purpose of computing the mean fluxes and ultimately constructing the difference image. The total numbers of valid and gapped in- and out-of-transit cadences are included in the DV output structure and in the figure caption for each difference image displayed in the DV report. Uncertainties in the mean in- and out-of-transit flux values for each transit are computed by standard methods under the assumption that the respective pixel values are not temporally correlated (i.e. correlated across cadences).

The overall mean in- and out-of-transit flux values are computed for each pixel by averaging the mean in- and out-of-transit levels associated with each of the transits over all of the transits in the target table. The difference image value for each pixel is then determined by subtracting the overall mean in-transit value from the overall mean out-of-transit value. Once again, uncertainties in the overall mean in- and out-of-transit flux values and in the difference value are computed by standard methods under the assumption that pixel values are not temporally correlated.

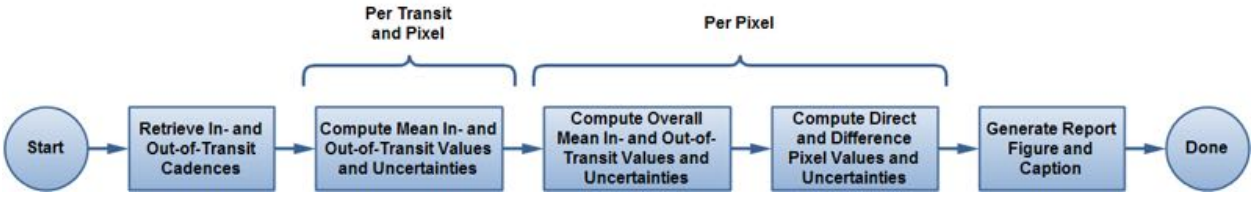

Figure 8: Formulation of in-transit, out-of-transit and difference images. Mean flux levels are computed in- and out-of-transit for each transit in the target table and then overall mean levels are computed by averaging over all transits in the target table. The flux difference for each pixel is determined by subtracting the overall mean in-transit value from the overall mean out-of-transit value respectively. The composite figure and caption are displayed for each planet candidate and target table (quarter) in the DV report for the associated target. A direct image and caption are displayed when a difference image cannot be generated for any reason.

An example illustrating the computation of the mean in- and out-of-transit values for one transit of Kepler-11e is shown in Figure 9. Fifty cadences are displayed from the time series associated with the brightest pixel in the optimal aperture of Kepler-11 in Q4. The out-of-transit cadences used to determine the mean out-of-transit flux level for this transit are marked in green. The mean out-of-transit value is displayed as a horizontal green line. Uncertainties in the mean out-of-transit flux level are shown in black above and below the mean level. Control cadences both preceding and following the transit permit meaningful averages and differences to be computed

without detrending (even for pixel time series with significant trends). The cadences used to determine the mean in-transit flux level are marked in red. The mean in-transit value is displayed as a horizontal red line with the associated uncertainties shown in black. The uncertainty in the mean out-of-transit value is less than that of the in-transit value because it is computed from a larger number of pixel values. The depth of this transit based on the out-of-transit level and difference shown here is 1350 ppm. The in- and out-of-transit cadences used to compute the mean levels for this transit were determined from the DV planet model fit to the corrected flux time series of this target for the observing quarters Q1-8.

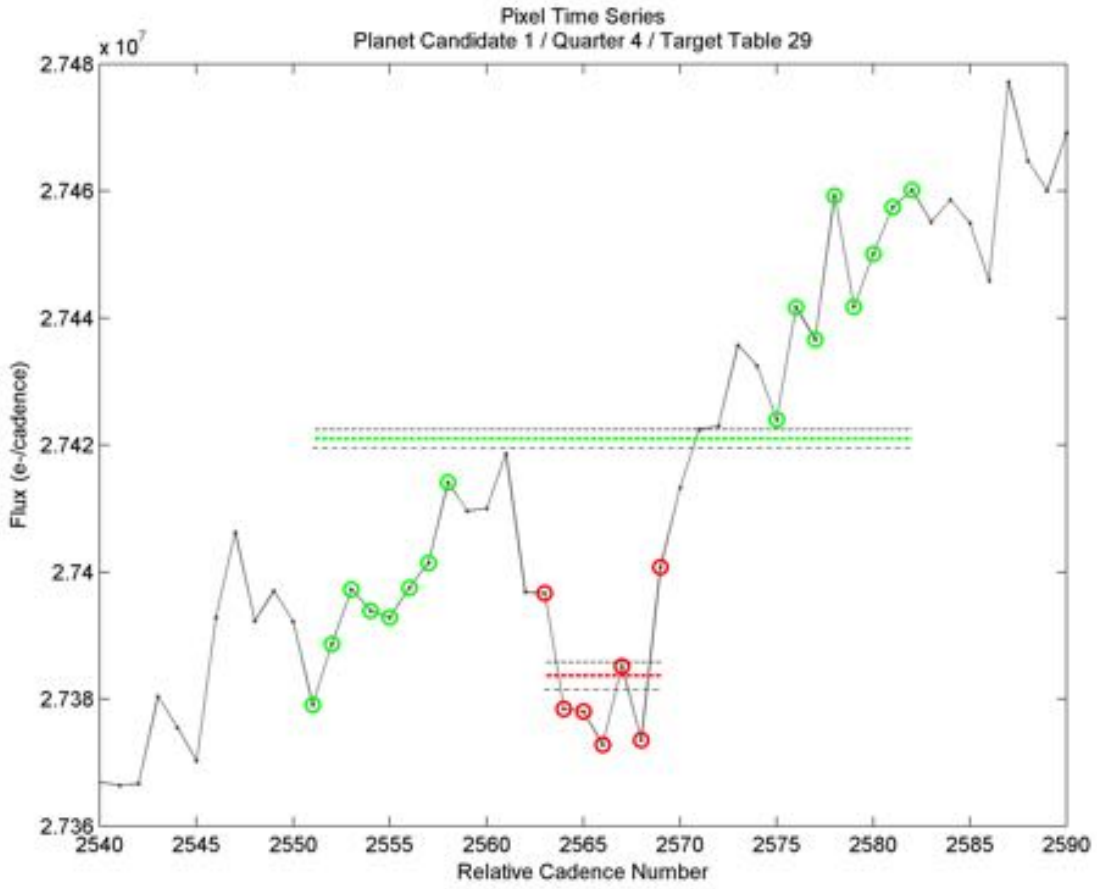

Figure 9: Time series for the brightest pixel in the optimal aperture of Kepler-11 in Q4. One transit of Kepler-11e is shown. The control cadences used to determine the out-of-transit mean flux level for this particular transit are marked in green. The mean out-of-transit value is displayed as a horizontal green line with associated one-sigma error bars in black. The cadences used to determine the in-transit mean flux level for this transit are marked in red. The mean in-transit flux level is displayed as a horizontal red line with associated error bars in black.

A second example illustrating the computation of mean in- and out-of-transit values for one transit of Kepler-11e is shown in Figure 10. Fifty cadences are displayed in this figure from the time series associated with a pixel just outside the optimal aperture of Kepler-11 in Q4. The pixel values are nearly two orders of magnitude smaller than those associated with the brightest pixel in the optimal aperture. It is clear that the mean in- and out-of-transit flux values for this transit agree within their respective uncertainties. This pixel is not sufficiently close to the location of Kepler-11 at the epoch of this transit to exhibit any evidence of Kepler-11e.

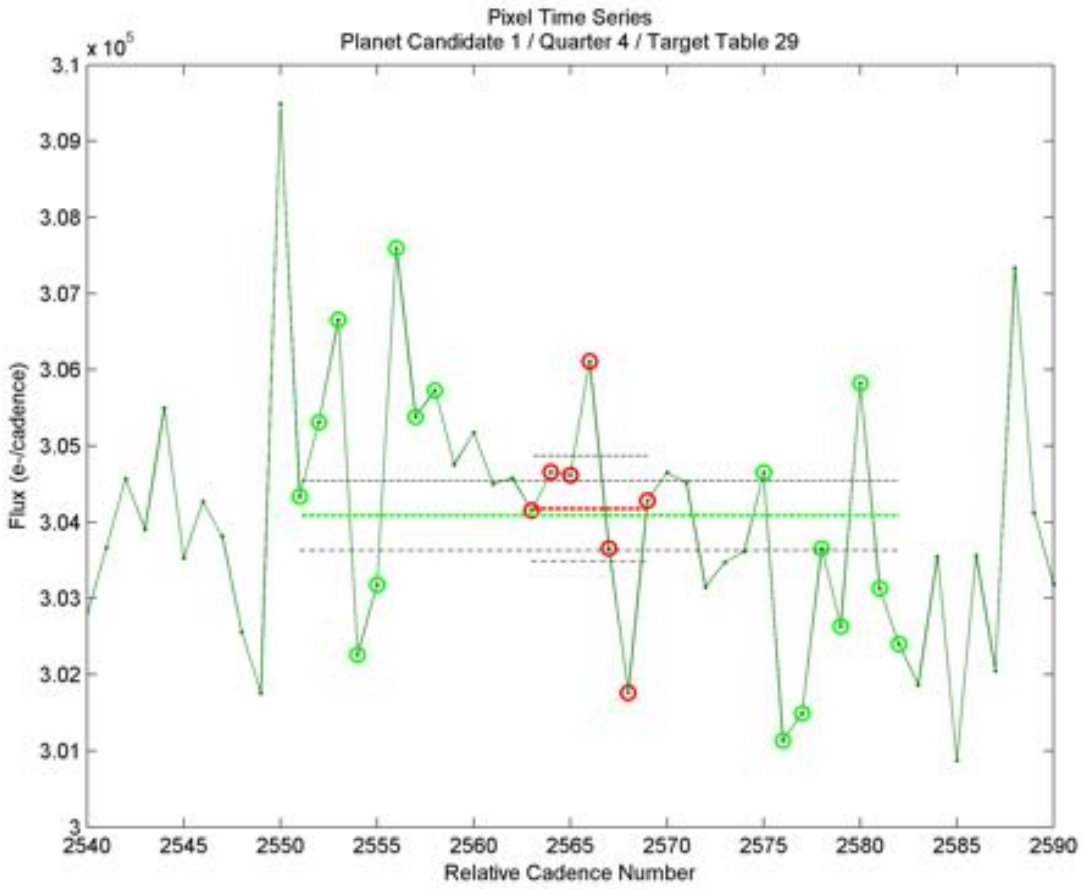

Figure 10: Time series for a pixel just outside the optimal aperture of Kepler-11 in Q4 (on the same cadences as the transit of Kepler-11e illustrated in Figure 9). Control cadences used to determine the mean out-of-transit flux level for this particular transit are marked in green. The mean out-of-transit value is displayed as a horizontal green line with associated one-sigma error bars in black. The cadences used to determine the mean in-transit flux level for this transit are marked in red. The mean in-transit flux level is displayed as a horizontal red line with associated error bars in black. The mean flux levels in- and out-of-transit agree within their respective uncertainties.

The DV difference image for Kepler-11e (KID 6541920) in Q5 is shown in Figure 11. The overall mean out-of-transit values are displayed in the upper right panel as a function of the CCD coordinates of the respective pixels in the target mask. The overall mean in-transit values are displayed in the lower left panel. The difference values are displayed in the upper left panel, and the difference SNR (values divided by uncertainties) is displayed in the lower right. The pixels in the target mask are outlined in each panel with a solid white line, and the pixels in the optimal aperture are outlined with a dashed white line.

Kepler-11e is a confirmed planet; it is the largest of the six known (as of this writing) transiting planets of Kepler-11. The scaling of the difference values is nearly three orders of magnitude less than that of the mean out-of-transit values, but the visual character of the figures displayed in the two upper panels is essentially identical. The reference position for this target based on its KIC coordinates is marked in all panels with an ‘x’; the centroid of the out-of-transit image is marked in the upper panels with a ‘+’; the centroid of the difference image is marked in the upper panels with a ‘Δ’. Centroiding of these images and centroid offset analysis will be discussed in the next section of this document. Nearby KIC objects are marked with asterisks in all panels and identified by Kepler ID and magnitude. The markers identifying KIC position and image centroids are closely packed; it is difficult to distinguish between transit source and target for this bona fide transiting planet.

The difference image for KOI 140 (KID 5130369) in Q3 is shown in Figure 12. KOI 140 is an astrophysical false positive (background eclipsing binary). The pixels with the largest flux differences for this planet candidate are clearly not coincident with the brightest pixels associated with the given target. In fact, the pixels with the largest flux differences do not even lie in the optimal aperture. The reference position for this target based on its KIC coordinates is marked in all panels with an ‘x’; the centroid of the out-of-transit image is marked in the upper panels with a ‘+’; the centroid of the difference image is marked in the upper panels with a ‘Δ’. Nearby KIC objects are marked with asterisks in all panels and identified by Kepler ID and magnitude. The transit source as identified by the centroid of the difference image is clearly offset from the position of the target as indicated by both the KIC reference position and the out-of-transit centroid. In fact, the centroid of the difference image is nearly coincident with the position of KID 5130380. This KIC object is 2.5 magnitudes (10 times) fainter than the given target and is almost certainly the source of the transit (i.e. eclipse) signature in the light curve of KOI 140.

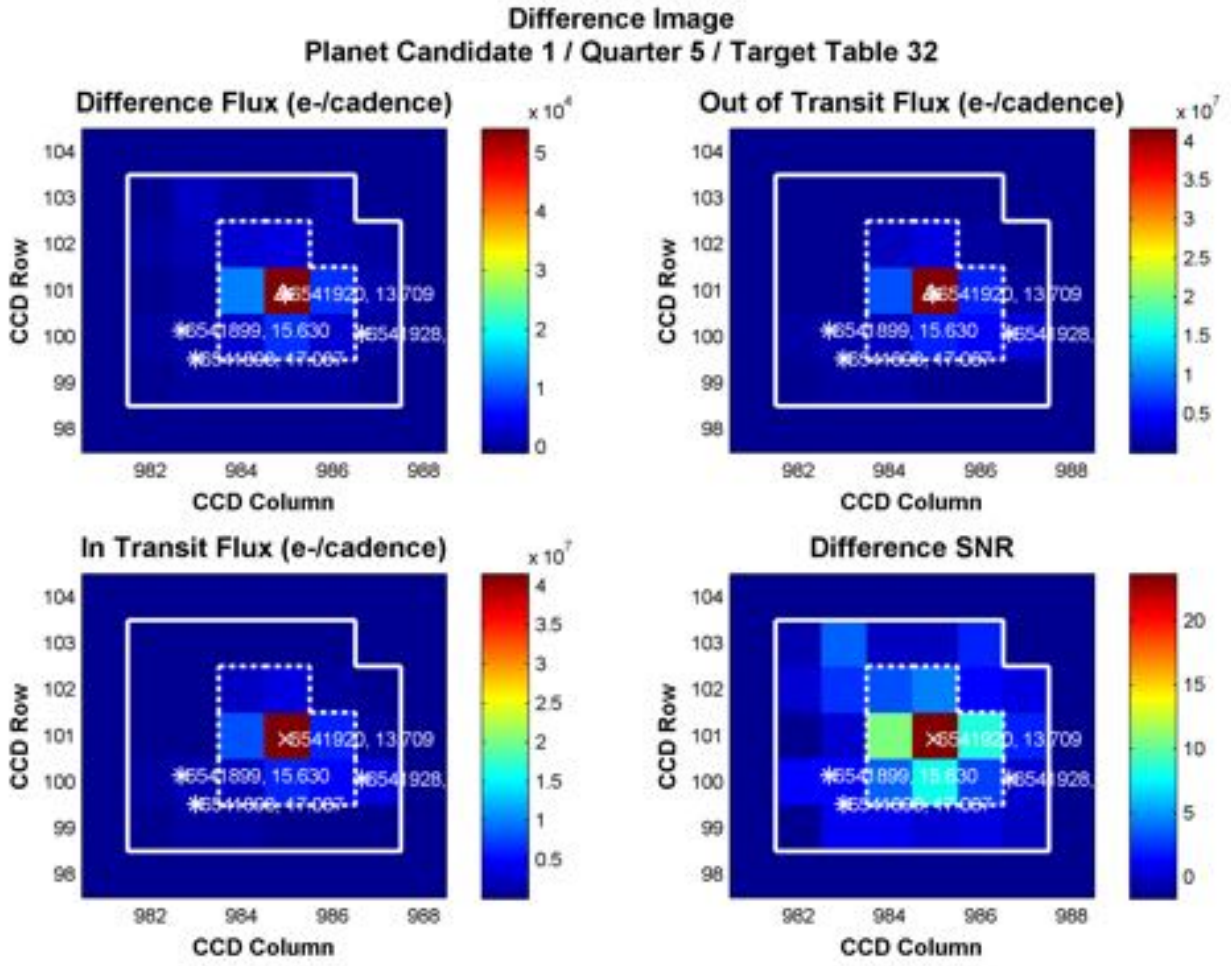

Figure 11: Difference image for Kepler-11e (KID 6541920) in Q5. The pixels in the target mask in this quarter are outlined in each panel with a solid white line. The pixels in the optimal aperture are outlined with a dashed white line. The mean out-of-transit values for the transit events in this target table are shown in the upper right panel, and the mean in-transit values are shown in the lower left panel. The difference values are displayed in the upper left panel, and the difference SNR (values divided by associated uncertainties) is shown in the lower right. Although the scaling of the difference values is nearly three orders of magnitude less than that of the mean out-of-transit values, the character of the images in both upper panels is essentially identical. It is difficult to distinguish between the transit source and the target itself. Kepler-11e is of course a confirmed transiting planet.

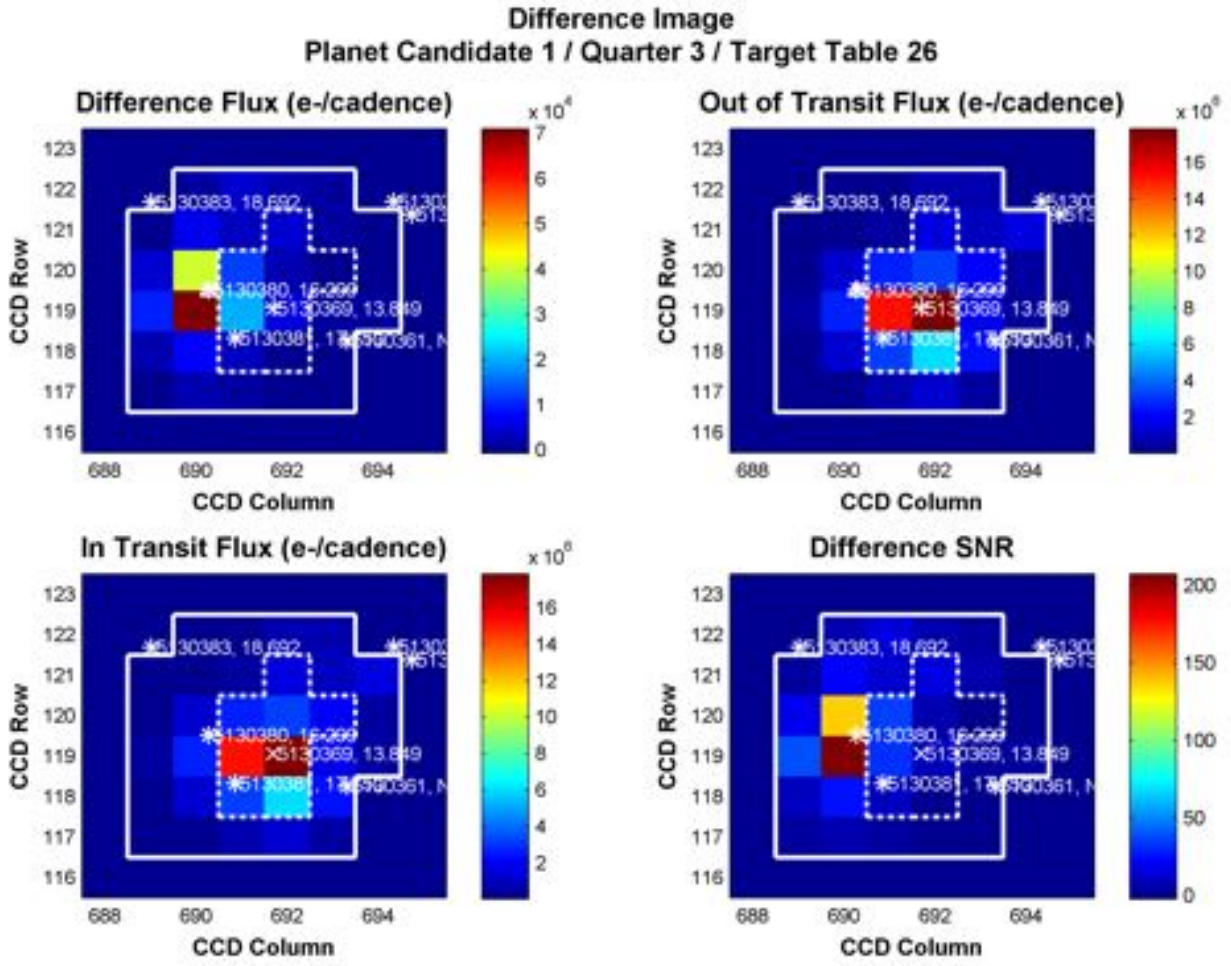

Figure 12: Difference image for KOI 140 (KID 5130369) in Q3. The pixels in the target mask in this quarter are outlined in each panel with a solid white line. The pixels in the optimal aperture are outlined with a dashed white line. The mean out-of-transit values for the transit events in this target table are shown in the upper right panel, and the mean in-transit values are shown in the lower left panel. The difference values are displayed in the upper left panel, and the difference SNR (values divided by associated uncertainties) is shown in the lower right. KOI 140 is an astrophysical false positive. The brightest pixels in the difference image are sufficiently offset from the location of the target that they lie outside of the optimal aperture. The location of the transit source as identified by the centroid of the difference image is nearly coincident with the position of KID 5130380.

2.3 Centroiding and Centroid Offset Analysis

Difference imaging is a powerful diagnostic for identifying false positive transiting planet detections. This is accomplished by taking advantage of the spatial information inherent in the

pixel time series to precisely locate the transit source in the photometric mask of the given target and determine the offset (in both absolute and statistical senses) between the transit source and the target itself. The target location is identified in DV by two different methods. Each method has associated advantages and disadvantages which will be discussed later. Offsets are subsequently computed with respect to each of the target locations. In cases where the results are significantly different, the DV consumer must decide which set of results (if any) to believe.

In the first case, the target CCD location is determined from its KIC right ascension and declination coordinates by evaluating *motion polynomials* and averaging over the **valid in-transit cadences** in the given target table. Motion polynomials are produced in PA by fitting the centroids of the ~200 PPA_STELLAR targets associated with each module output on a cadence by cadence basis. The motion polynomials therefore provide a measured mapping between right ascension and declination coordinates on the sky and CCD row and column coordinates on the focal plane. Evaluating the motion polynomials on the in-transit cadences and averaging the results allows the mean focal plane position of the target to be determined over the clean transits in the given target table (recall that the target position on the focal plane is not static, but changes dynamically due to differential velocity aberration, focus variations, pointing variations and such). The uncertainties in the row and column coordinates for the KIC reference position are given by the RMS uncertainty in the per cadence row and column estimates. Averaging over many cadences is performed because the target is not stationary in the reference frame of the focal plane; it is not performed to reduce the uncertainty in the CCD coordinate estimates. The row and column coordinate estimates are **assumed** to be independent because the motion polynomials are separately computed in PA from row and column PPA_STELLAR centroid coordinates and therefore do not support the determination of row/column covariance relationships.

In the second case, the target location on the CCD is determined for each target table by computing the PRF-based centroid of the out-of-transit control image. The centroid aperture includes all pixels in the target mask (as of DV 8.0). PRF-based centroiding is performed by calling a library of functions that is shared with the PA and PDQ CSCIs. The centroiding library will be the subject of a separate Design Note and will not be discussed here. The process essentially involves solving for row/column translations (and scaling) of the Pixel Response Function for the given module output that best fit the pixel values in the out-of-transit image. The centroid library functionality produces a row/column covariance matrix for each centroid so propagation of centroid uncertainties to later offset computations is not performed under the assumption that row and column coordinates are independent.

The KIC focal plane reference positions and associated uncertainties are included in the DV output structure per planet candidate and target table. In addition, the positions are marked with the character ‘x’ on each of the difference image panels as shown in Figure 11 and Figure 12. The KIC celestial location is also included in the DV output structure (per planet candidate and target table). In this case the right ascension and declination coordinates have no uncertainty. PRF-based out-of-transit image centroids and associated uncertainties are likewise included in the DV output structure per planet candidate and target table. They are marked with the

character '+' on the upper difference image panels as shown in Figure 11 and Figure 12. PRF-based out-of-transit centroids are transformed to sky coordinates by inverting motion polynomials and averaging over the valid in-transit cadences for the given target table. The sky coordinates and associated uncertainties are populated in the DV output structure per planet candidate and target table. The covariance matrix for the transformed sky coordinates is determined as the mean of the per cadence RA/Dec covariance matrices.

The location of the transit source is determined for each planet candidate and target table by computing the PRF-based centroid of the difference image. As before, the centroid is transformed to sky coordinates with associated uncertainties. The difference image centroid is marked with the character 'Δ' on the upper difference image panels as shown in Figure 11 and Figure 12. The centroid values and uncertainties in both focal plane and sky coordinates are included in the DV output structure for all planet candidates and target tables.

Once the target and transit source locations have been computed, the centroid offsets are determined on both focal plane (in units of pixels) and sky (in units of arcseconds). The process is illustrated in Figure 13. The magnitude of the offset (i.e. *offset distance*) is computed in each case as the quadrature sum of the two offset components. The uncertainty in the magnitude of each offset is computed by standard propagation of uncertainty methods. All centroid offsets, offset distances and associated uncertainties are included in the DV output structure for each planet candidate and target table. It should be noted that if the difference image centroid cannot be successfully determined for a given planet candidate and target table then none of the centroid offsets are computed either. Furthermore, if the difference image centroid is successfully computed but the out-of-transit centroid is not then the centroid offsets are only determined with respect to the KIC reference position.

The magnitude of the centroid offsets provides both absolute and statistical (i.e. number of standard deviations) measures of the separation between the target and the transit source (which may of course be the target itself). If the offset magnitude is small then the viability of the planet candidate is significant; it may be the case that there is a background object (transiting or eclipsing) close to the target but it is not likely the case that there is such a background object well separated from the target. If the offset magnitude is large then the viability of the planet candidate must be called into question; it is likely that there is a background object well separated from the target.

As stated earlier, there are advantages and disadvantages associated with computing the centroid offsets with respect to each of the target locations described earlier. These must be understood to properly interpret the computed offsets. The out-of-transit image centroid is subject to crowding in the target aperture whereas the difference image centroid is not. In a crowded aperture it is therefore possible to obtain a significant offset with respect to the out-of-transit centroid even for a true transiting planet candidate. The KIC reference position is not subject to crowding (to the extent of course that KIC coordinates are not subject to crowding), but the centroid offset with respect to the KIC position is subject to biases or errors in the PRF centroiding process itself. These errors tend to cancel when the offset is computed between

PRF-based centroids for both out-of-transit and difference images, but the errors do not tend to cancel when the offset computation involves only one PRF-based centroid.

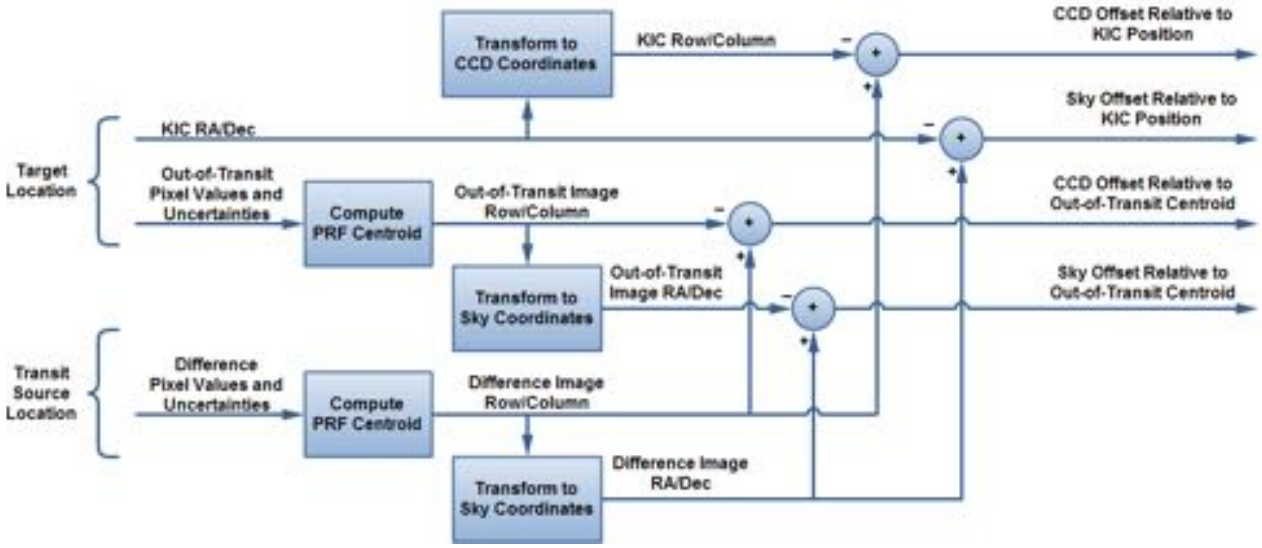

Figure 13: Centroid offset computation. Offsets of the transit source location (difference image centroid) are computed with respect to each of the target locations (KIC reference position and out-of-transit centroid) on both focal plane and sky.

An example illustrating the difference image centroid offsets for Kepler-11e is presented in Figure 14. The offsets of the quarterly difference image centroid relative to the out-of-transit image centroid are displayed in green in the left panel. The error bars indicate the one-sigma uncertainties in right ascension and declination for each offset. The offsets are also marked with the quarterly data set ('Qn') from which they were computed. The quarterly offsets with respect to the KIC position of the target are displayed in the same fashion in the right panel.

The robust weighted (by inverse uncertainties) mean offset over the eight quarterly data sets is displayed in each panel in magenta with associated error bars. The three-sigma *radius of confusion* (i.e. three times the uncertainty in the magnitude of the mean offset) is displayed in each panel in blue. The target is located at the origin in each panel which lies comfortably within the respective radii of confusion. The transit source cannot be statistically differentiated from the target itself in each case. Kepler-11e is of course a confirmed transiting planet. The Q5 difference image for this target was shown in Figure 11. Robust (to deemphasize outliers) averaging of multiple quarterly offsets improves the accuracy of the estimate of transit source location. The magnitude derived from the mean right ascension and declination offsets is 0.0798 $\pm$ 0.0802 arcseconds (0.99 sigma) with respect to the out-of-transit centroid, and 0.1425 $\pm$ 0.0963 arcseconds (1.48 sigma) with respect to the KIC position of the target.

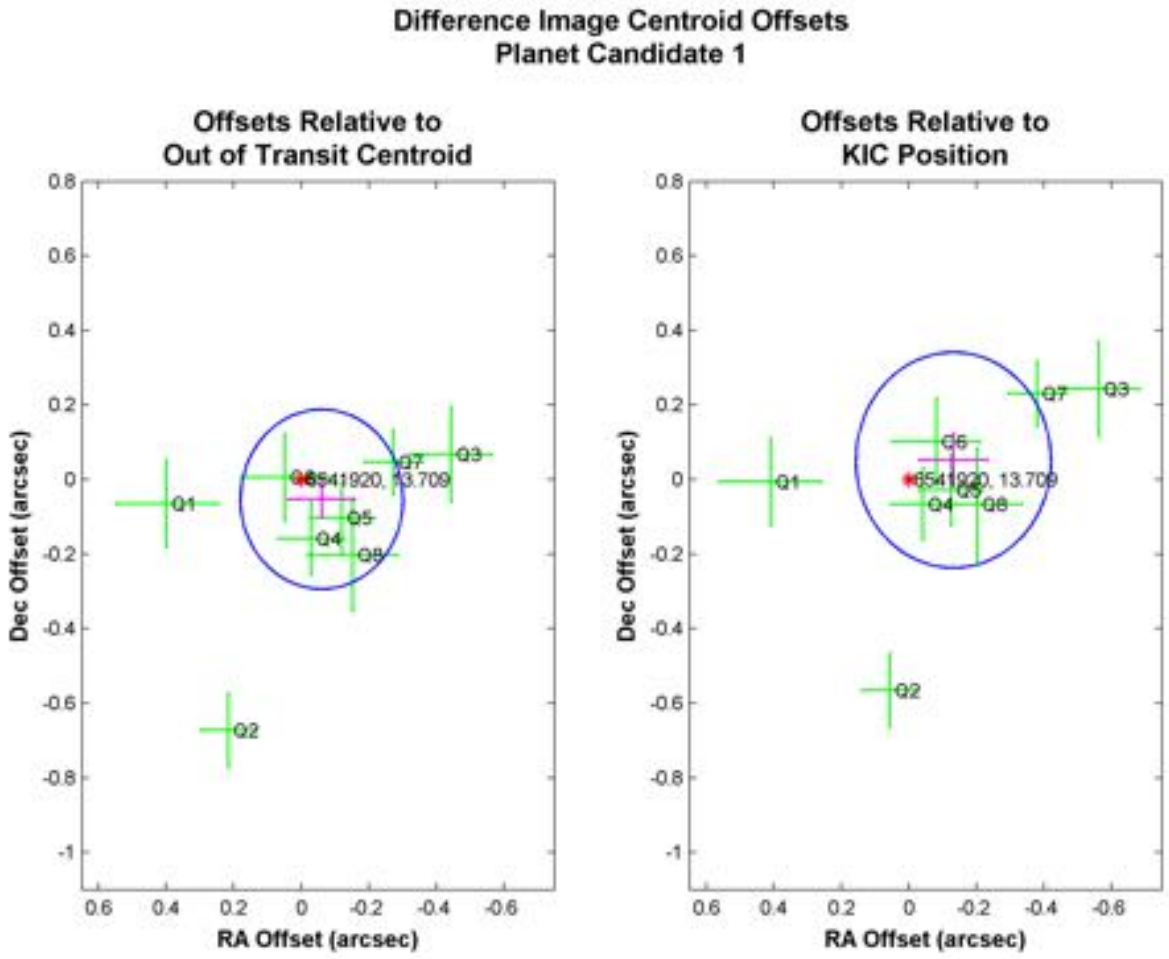

Figure 14: Difference image centroid offsets for Kepler-11e. The quarterly centroid offsets in right ascension and declination with respect to the out-of-transit centroids are shown in the left panel in green. The error bars indicate one-sigma uncertainties. Each offset is marked with the quarterly data set from which it was computed. The quarterly centroid offsets with respect to the KIC target location are shown in the right panel. The robust mean offset over Q1-8 is shown with associated error bars in each figure in magenta; the three-sigma radii of confusion for the mean offsets are shown in blue. The target is located at the origin (0, 0) in each panel and marked with a red asterisk.

An example illustrating the difference image centroid offsets for KOI 140 is shown in Figure 15. It is interesting that outlier offsets in both cases are associated with the same seasonal orientation of the photometer (Q1/Q5). The target is located at the origin in the offset reference frame which lies well outside the respective radii of confusion. KOI 140 is an astrophysical false positive (background eclipsing binary). The Q3 difference image for this target was shown in Figure 12. The magnitude derived from the mean right ascension and declination offsets is

5.806 $\pm$ 0.040 arcseconds (147 sigma) with respect to the out-of-transit centroid, and 5.867 $\pm$ 0.031 arcseconds (190 sigma) with respect to the KIC position of the target. The robust mean offset in each panel hints strongly that the true source of the transit signature for this candidate is KID 5130380 which is 2.5 magnitudes fainter than the given target.

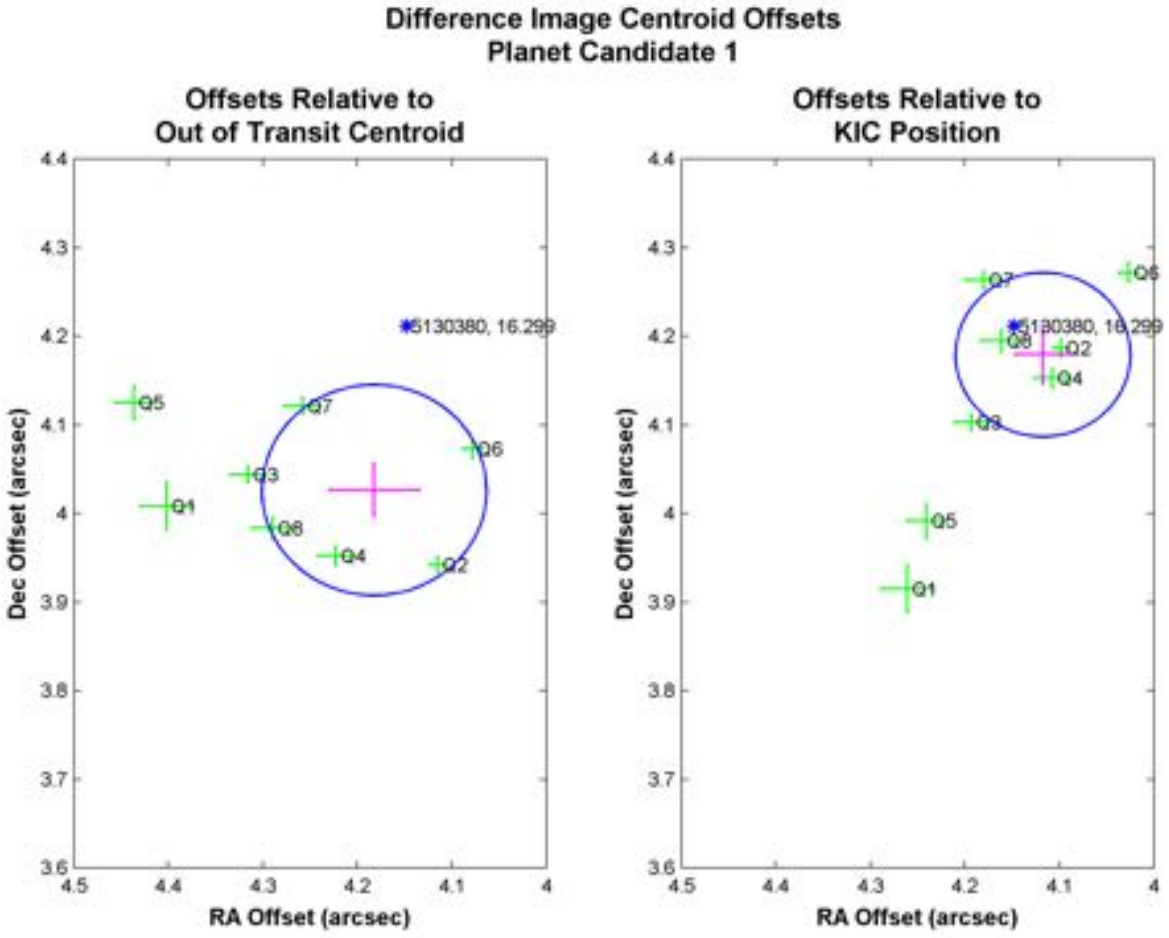

Figure 15: Difference image centroid offsets for KOI 140 (KID 5130369). The quarterly centroid offsets in right ascension and declination with respect to the out-of-transit centroids are shown in the left panel in green. The error bars indicate one-sigma uncertainties. Each offset is marked with the quarterly data set from which it was computed. The quarterly centroid offsets with respect to the KIC reference target location are shown in the right panel. The robust mean offset over Q1-8 is shown with associated error bars in each figure in magenta; the three-sigma radii of confusion for the mean offsets are shown in blue. The target is located at the origin in the offset reference frame and does not appear in either panel; KOI 140 is an astrophysical false positive. The true source of the transit signature is likely to be KID 5130380 which is marked in each panel with a blue asterisk.

3. Difference Image Module Parameters

The module parameters pertaining to DV difference imaging are defined in this section. Data types, units and (SOC 8.0) default values are specified. The values of these parameters may be modified by the SOC operator (within acceptable validation limits) when the DV pipeline is launched. There is an additional DV parameter (`differenceImageGenerationEnabled`) which determines whether or not the difference image generation code is actually executed when DV is launched. The default value for this parameter is true. This parameter was added to the module interface primarily to support DV development and testing.

Parameter Name	Type	Units	Default	Description
`anomalyBufferInDays`	Float	Days	1.0	Length of data segment following Earth-points and safe modes for exclusion of individual transits from difference images
`controlBufferInCadences`	Integer	Cadences	3	Length of cadence buffer to insert between transits and associated out-of-transit control segments
`minInTransitDepth`	Float		0.75	Minimum depth as fraction of transit depth for identification of in-transit cadences
`detrendingEnabled`	Logical		False	If true, perform detrending of all pixel time series prior to generation of difference images
`detrendPolyOrder`	Integer		2	Polynomial order for initial detrending stage
`defaultMedianFilterLength`	Integer	Cadences	73	Median filter length for detrending if length cannot be determined from planet model fit parameters
`boundedBoxWidth`	Float	Arcseconds	64.0	Dimension of bounded box in RA and Dec centered on the target for which nearby KIC objects are included in the module interface for placement on difference images

Table 1: Difference image parameter set. The values for these parameters may be modified by the SOC operator prior to launching the DV pipeline.

4. Derivations

Mathematical details underlying the formulation of the difference images and propagation of the associated uncertainties are presented in 4.1. Mathematical details underlying the computation of the centroid offsets, robust averaging of the offsets over multiple quarters and propagation of the associated uncertainties are presented in 4.2.

4.1 Difference Image Formulation

For each pixel in the target aperture mask, let u_{ij} and $\sigma_{u_{ij}}$ denote the pixel value and uncertainty for the j^{th} in-transit cadence associated with transit i in a given target table. Furthermore, let N_{u_i} denote the number of valid (i.e. ungapped) in-transit cadences for the i^{th} transit. Likewise, let v_{ij} and $\sigma_{v_{ij}}$ denote the pixel value and uncertainty for the j^{th} out-of-transit cadence associated with transit i, and let N_{v_i} denote the number of valid out-of-transit cadences for the i^{th} transit. The mean in- and out-of-transit values associated with the i^{th} transit are denoted by $\bar{u}_i$ and $\bar{v}_i$ respectively for each pixel, and may be computed as follows:

$$\bar{u}_i = \frac{1}{N_{u_i}} \sum_{j=1}^{N_{u_i}} u_{ij}$$

$$\bar{v}_i = \frac{1}{N_{v_i}} \sum_{j=1}^{N_{v_i}} v_{ij}$$

The uncertainties associated with the mean in- and out-of-transit values for the i^{th} transit are denoted by $\sigma_{\bar{u}_i}$ and $\sigma_{\bar{v}_i}$. Under the assumption that the respective pixel values are not temporally correlated, the uncertainties in the mean values for each transit are determined by:

$$\sigma_{\bar{u}_i} = \sqrt{\frac{1}{{N_{u_i}}^2} \sum_{j=1}^{N_{u_i}} {\sigma_{u_{ij}}}^2}$$

$$\sigma_{\bar{v}_i} = \sqrt{\frac{1}{{N_{v_i}}^2} \sum_{j=1}^{N_{v_i}} {\sigma_{v_{ij}}}^2}$$

For each pixel, the overall mean in- and out-of-transit flux values are denoted by $\bar{u}$ and $\bar{v}$. The overall mean levels are obtained by averaging over all transits in the target table as follows:

$$\bar{u} = \frac{1}{N_t} \sum_{i=1}^{N_t} \bar{u}_i$$

$$\bar{v} = \frac{1}{N_t} \sum_{i=1}^{N_t} \bar{v}_i$$

The number of (clean) transits in the target table is denoted N_t. Let the uncertainties associated with the overall mean in- and out-of-transit values be denoted by $\sigma_{\bar{u}}$ and $\sigma_{\bar{v}}$ respectively. These are computed under the assumption of independence discussed earlier by:

$$\sigma_{\bar{u}} = \sqrt{\frac{1}{{N_t}^2} \sum_{i=1}^{N_t} {\sigma_{\bar{u}_i}}^2}$$

$$\sigma_{\bar{v}} = \sqrt{\frac{1}{{N_t}^2} \sum_{i=1}^{N_t} {\sigma_{\bar{v}_i}}^2}$$

Finally, let the difference flux value and uncertainty for each pixel in the target mask be denoted by Δf and $\sigma_{\Delta f}$ respectively. The difference value and uncertainty are computed as follows:

$$\Delta f = \bar{v} - \bar{u}$$

$$\sigma_{\Delta f} = \sqrt{{\sigma_{\bar{u}}}^2 + {\sigma_{\bar{v}}}^2}$$

4.2 Centroid Offset Analysis

Let (x_t, y_t) represent the focal plane CCD coordinates of the given target, and let (x_s, y_s) denote the focal plane coordinates of the transit source. The focal plane offsets Δx and Δy are then determined by:

$$\Delta x = x_s - x_t$$

$$\Delta y = y_s - y_t$$

The offset distance d between transit source and target is the quadrature sum of the individual offset components and may be computed as follows:

$$d = \sqrt{\Delta x^2 + \Delta y^2}$$

The focal plane offsets and offset distance are computed in DV in units of pixels. As described earlier, the transit source location is determined by the difference image centroid for each target table. The target location is determined either by the KIC reference position or the out-of-transit image centroid for each target table.

Uncertainties in the focal plane offsets and offset distance are propagated by standard methods from the covariance matrices $C_{x_t y_t}$ and $C_{x_s y_s}$ for the target and source coordinates respectively based on Jacobian transformations associated with the offset functions. The Jacobian transformations for computation of the offsets Δx and Δy and offset distance d are denoted by $J_{\Delta x}$, $J_{\Delta y}$ and J_d respectively, and may be described with respect to the target and source coordinates by four-element row vectors as follows:

$$J_{\Delta x} = \left[\frac{\partial \Delta x}{\partial x_t} \quad \frac{\partial \Delta x}{\partial y_t} \quad \frac{\partial \Delta x}{\partial x_s} \quad \frac{\partial \Delta x}{\partial y_s}\right] = [\,-1 \quad 0 \quad 1 \quad 0\,]$$

$$J_{\Delta y} = \left[\frac{\partial \Delta y}{\partial x_t} \quad \frac{\partial \Delta y}{\partial y_t} \quad \frac{\partial \Delta y}{\partial x_s} \quad \frac{\partial \Delta y}{\partial y_s}\right] = [\,0 \quad -1 \quad 0 \quad 1\,]$$

$$J_d = \left[\frac{\partial d}{\partial x_t} \quad \frac{\partial d}{\partial y_t} \quad \frac{\partial d}{\partial x_s} \quad \frac{\partial d}{\partial y_s}\right] = \frac{[\,-\Delta x \quad -\Delta y \quad \Delta x \quad \Delta y\,]}{d}$$

Given the covariance matrices for the target and source coordinates and the Jacobian transformations as defined above, the uncertainties in the focal plane offsets and offset distance are computed as follows:

$$\sigma_{\Delta x} = \sqrt{J_{\Delta x} * C_{xy} * J_{\Delta x}{}'}$$

$$\sigma_{\Delta y} = \sqrt{J_{\Delta y} * C_{xy} * J_{\Delta y}{}'}$$

$$\sigma_d = \sqrt{J_d * C_{xy} * J_d{}'}$$

where the covariance matrix describing the target and transit source coordinates is defined by:

$$C_{xy} = \begin{bmatrix} C_{x_t y_t} & 0 \\ 0 & C_{x_s y_s} \end{bmatrix}$$

The uncertainties in the row and column offsets reduce to:

$$\sigma_{\Delta x} = \sqrt{{\sigma_{x_t}}^2 + {\sigma_{x_s}}^2}$$

$$\sigma_{\Delta y} = \sqrt{{\sigma_{y_t}}^2 + {\sigma_{y_s}}^2}$$

where ${\sigma_{x_t}}^2$ and ${\sigma_{y_t}}^2$ are the diagonal elements of $C_{x_t y_t}$ (i.e. variances associated with the focal plane coordinates of the target), and ${\sigma_{x_s}}^2$ and ${\sigma_{y_s}}^2$ are the diagonal elements of $C_{x_s y_s}$.

If the off-diagonal elements of $C_{x_t y_t}$ and $C_{x_s y_s}$ are identically zero (i.e. the row and column coordinates for the target and the transit source locations are uncorrelated), the uncertainty in the focal plane offset distance reduces to:

$$\sigma_d = \sqrt{\frac{\Delta x^2 {\sigma_{\Delta x}}^2 + \Delta y^2 {\sigma_{\Delta y}}^2}{d^2}}$$

The situation regarding centroid offsets and offset distance in sky coordinates is more complicated. In the equatorial coordinate system, the offset in right ascension must include a declination cosine factor. Let (α_t, δ_t) represent the right ascension and declination coordinates of the given target, and let (α_s, δ_s) denote the right ascension and declination coordinates of the transit source. The sky offsets $\Delta\alpha$ and $\Delta\delta$ are then determined by:

$$\Delta\alpha = (\alpha_s - \alpha_t)\cos\delta_t$$

$$\Delta\delta = \delta_s - \delta_t$$

The offset distance between transit source and target is denoted by θ and computed as follows:

$$\theta = \sqrt{\Delta\alpha^2 + \Delta\delta^2}$$

The sky offsets and offset distance are computed in DV in units of arcseconds. Uncertainties in the sky offsets and offset distance are propagated by standard methods from the covariance matrices $C_{\alpha_t \delta_t}$ and $C_{\alpha_s \delta_s}$ for the target and source coordinates respectively based on Jacobian

transformations associated with the offset functions. The Jacobian transformations for computation of the offsets $\Delta\alpha$ and $\Delta\delta$ and the offset distance θ are denoted by $J_{\Delta\alpha}$, $J_{\Delta\delta}$ and J_θ respectively, and may be described with respect to the target and source coordinates by four-element row vectors as follows:

$$J_{\Delta\alpha} = \left[\frac{\partial\Delta\alpha}{\partial\alpha_t} \quad \frac{\partial\Delta\alpha}{\partial\delta_t} \quad \frac{\partial\Delta\alpha}{\partial\alpha_s} \quad \frac{\partial\Delta\alpha}{\partial\delta_s}\right] = \left[-\cos\delta_t \quad -(\alpha_s - \alpha_t)\sin\delta_t \quad \cos\delta_t \quad 0\right]$$

$$J_{\Delta\delta} = \left[\frac{\partial\Delta\delta}{\partial\alpha_t} \quad \frac{\partial\Delta\delta}{\partial\delta_t} \quad \frac{\partial\Delta\delta}{\partial\alpha_s} \quad \frac{\partial\Delta\delta}{\partial\delta_s}\right] = \left[0 \quad -1 \quad 0 \quad 1\right]$$

$$J_\theta = \left[\frac{\partial\theta}{\partial\alpha_t} \quad \frac{\partial\theta}{\partial\delta_t} \quad \frac{\partial\theta}{\partial\alpha_s} \quad \frac{\partial\theta}{\partial\delta_s}\right] = \frac{\left[-\Delta\alpha\cos\delta_t \quad -\Delta\alpha(\alpha_s - \alpha_t)\sin\delta_t - \Delta\delta \quad \Delta\alpha\cos\delta_t \quad \Delta\delta\right]}{\theta}$$

Given the covariance matrices for the target and source coordinates and the Jacobian transformations as defined above, the uncertainties in the sky offsets and offset distance are computed as follows:

$$\sigma_{\Delta\alpha} = \sqrt{J_{\Delta\alpha} * C_{\alpha\delta} * J_{\Delta\alpha}{}'}$$

$$\sigma_{\Delta\delta} = \sqrt{J_{\Delta\delta} * C_{\alpha\delta} * J_{\Delta\delta}{}'}$$

$$\sigma_\theta = \sqrt{J_\theta * C_{\alpha\delta} * J_\theta{}'}$$

where the covariance matrix describing the target and transit source locations is defined by:

$$C_{\alpha\delta} = \begin{bmatrix} C_{\alpha_t\delta_t} & 0 \\ 0 & C_{\alpha_s\delta_s} \end{bmatrix}$$

If the target declination δ_t is equal to zero, the derivations of sky offsets, offset distance and associated uncertainties are equivalent to those of the related focal plane offsets and uncertainties. The declination cosine is identically equal to one in this case and the declination sine is identically equal to zero.

The quarterly offsets in right ascension and declination are robustly averaged independently. If `raOffsetValues` is a column vector of the quarterly right ascension offsets with uncertainties `raOffsetUncertainties` then the robust weighted mean right ascension offset and associated uncertainty are computed with the Matlab `robustfit` function by:

```
[meanRaOffsetValue, stats] = robustfit( ...
    1 ./ raOffsetUncertainties, ...
```

```
    raOffsetValues ./ raOffsetUncertainties, ...
    [], ...
    [], ...
    'off');
meanRaOffsetUncertainty = stats.se;
```

The quarterly declination offsets are robustly averaged in the same fashion:

```
[meanDecOffsetValue, stats] = robustfit( ...
    1 ./ decOffsetUncertainties, ...
    decOffsetValues ./ decOffsetUncertainties, ...
    [], ...
    [], ...
    'off');
meanDecOffsetUncertainty = stats.se;
```

The design "matrix" and the vector of quarterly offset values are each weighted by the inverse of the respective uncertainties in the quarterly offsets for the purpose of robustly estimating the weighted mean.

In the nomenclature defined earlier, the mean right ascension and declination offsets $\overline{\Delta\alpha}$ and $\overline{\Delta\delta}$ may equivalently be computed from the final robust weights $w_{\Delta\alpha_i}$ and $w_{\Delta\delta_i}$ as follows:

$$\overline{\Delta\alpha} = \sum_{i=1}^{N_q} \left(w_{\Delta\alpha_i} / {\sigma_{\Delta\alpha_i}}^2 \right) \Delta\alpha_i \Big/ \sum_{i=1}^{N_q} \left(w_{\Delta\alpha_i} / {\sigma_{\Delta\alpha_i}}^2 \right)$$

$$\overline{\Delta\delta} = \sum_{i=1}^{N_q} \left(w_{\Delta\delta_i} / {\sigma_{\Delta\delta_i}}^2 \right) \Delta\delta_i \Big/ \sum_{i=1}^{N_q} \left(w_{\Delta\delta_i} / {\sigma_{\Delta\delta_i}}^2 \right)$$

where the number of quarterly offsets is denoted by N_q.

The uncertainties $\sigma_{\overline{\Delta\alpha}}$ and $\sigma_{\overline{\Delta\delta}}$ returned by `robustfit` are not based simply on the linear transformations for $\overline{\Delta\alpha}$ and $\overline{\Delta\delta}$, but also represent the spread in the quarterly offsets $\Delta\alpha_i$ and $\Delta\delta_i$ respectively. The mean sky offset distance $\bar{\theta}$ and associated uncertainty $\sigma_{\bar{\theta}}$ are computed from the mean right ascension and declination offsets and uncertainties by:

$$\bar{\theta} = \sqrt{\overline{\Delta\alpha}^2 + \overline{\Delta\delta}^2}$$

$$\sigma_{\bar{\theta}} = \sqrt{\frac{\overline{\Delta\alpha}^2 \sigma_{\overline{\Delta\alpha}}^2 + \overline{\Delta\delta}^2 \sigma_{\overline{\Delta\delta}}^2}{\bar{\theta}^2}}$$